Proton Radiation Effects on HgCdTe Avalanche Photodiode Detectors

Xiaoli Sun, *Member, IEEE*, James B. Abshire, Jean-Marie Lauenstein, *Member, IEEE*, Sachidananda R. Babu, *Member, IEEE*, Jeff D. Beck, *Member, IEEE*, William W. Sullivan III, *Member, IEEE*, and John E. Hubbs, *Member, IEEE*

***Abstract*— Space radiation damage and proton-induced transient effects were evaluated on 4.4-μm cutoff HgCdTe avalanche photodiode (APD) arrays developed by Leonardo DRS. Device performances as a function of total dose up to 100 krad (Si) were measured with ∼60-MeV protons on three types of APD samples: 4 × 4 pixel APD fanout arrays with and without connection to a read-out integrated circuit (ROIC) and a 2 × 8 pixel photon-counting APD focal plane array (FPA). A gamma-ray test was also conducted to study ionization effects. Both APD arrays exhibited a small decrease in the quantum efficiency and a linear increase in the dark current with the proton fluence. The 2 × 8 pixel photon-counting FPA also exhibited an increase in the dark count rate with proton dose. After the proton irradiation and an overnight room-temperature warm-up, the APD dark currents at 80 K increased significantly in both types of APD arrays. All radiation damage to these HgCdTe APD arrays annealed out after baking them at >85 °C for several hours. Transient protons through the devices were found to cause large pulses at the detector output, but recover within 1 μs.**

***Index Terms*— HgCdTe avalanche photodiodes (APDs), infrared detectors, lidar, radiation damage.**

I. Introduction

HgCdTe photodiode arrays have been used as imaging sensors in space from the short-wave infrared (SWIR) to mid-wave infrared (MWIR) wavelength region [1]–[3]. HgCdTe avalanche photodiode (APD) arrays with linear analog waveform outputs and single-photon sensitivity have recently been developed [4]–[14]. The maximum APD gain ranges from tens to thousands with near-unity excess noise factor. As a result, the photocurrents from the APDs can override the electronic noise in high-bandwidth read-out circuits. They give linear analog pulse waveform outputs with a few nanosecond response times and a subphoton noise level.

NASA Goddard Space Flight Center (GSFC) has collaborated with Leonardo DRS Electro-Optical Infrared Systems to develop HgCdTe APD arrays for space lidar receivers. Two types of HgCdTe APD focal plane arrays (FPAs) have been developed: 4 × 4 pixel HgCdTe APD arrays with 80 μm × 80 μm pixel size for trace gas lidar [15], [16] and 2 × 8 pixel linear mode photon-counting (LMPC) HgCdTe APD arrays with 64 μm × 64 μm pixel size as precursor detector systems for swath mapping lidar [17]–[19]. The quantum efficiency of these detectors can be tailored to be >90% from 0.9 to 4.3 μm by proper antireflection (AR) coating and HgCdTe thickness adjustment. The gain normalized dark current at 80 K is as low as 4.8 fA per pixel, or 120 pA/cm^2, at APD gains as high as 1900 [18]. The devices can operate from 77 to 115 K with nearly the same performance [16]. These characteristics enable new classes of airborne and space-based lidar for Earth and planetary science investigations from near-infrared to MWIR wavelengths [20].

For space applications, it is important to understand the effects of radiation on these devices. Radiation damage of HgCdTe photodiode arrays without avalanche gain have been studied extensively [21]–[28] and the results show that they are much less susceptible to radiation damage than their silicon counterparts [29]–[31]. However, due to the relatively high electron multiplication gain, HgCdTe APDs are expected to be more susceptible to space radiation damage.

We have conducted a series of radiation damage tests on the HgCdTe APD arrays developed by DRS to the radiation levels of typical multiyear low-Earth orbital missions [32]. Protons were used to characterize displacement damage and total ionizing dose (TID) radiation effects. Gamma rays were used to study the effects of TID without the displacement damage. Transient response measurements were performed under 60-MeV proton irradiation. The annealing characteristics of the APDs were characterized through a series of heating and cooling cycles. Some of the test results have been presented at SPIE Infrared Technology and Application XLIV in 2018 [33]. A more careful and comprehensive analysis of the test data has recently been conducted, which helped to understand the test results and, in some cases, correct our early conclusions. This article gives a more clear and concise description of the test setup and the findings from the updated data analysis.

Manuscript received November 4, 2020; revised November 22, 2020; accepted November 23, 2020. Date of publication November 26, 2020; date of current version January 19, 2021. This work was supported in part by the NASA Earth Science Technology Office through the Instrument Incubator Program under Grant IIP-10-0035, in part by the In-Space Validation of Earth Science Technology under Grant InVEST-12-0023, and in part by the Advanced Technology Initiatives under Grant ATI-QRS-15-008 and Grant ATI-QRS-17-0001.

Xiaoli Sun, James B. Abshire, and Jean-Marie Lauenstein are with National Aeronautics and Space Administration, Goddard Space Flight Center, Greenbelt, MD 20771 USA (email: xiaoli.sun-1@nasa.gov).

Sachidananda R. Babu is with NASA, Earth Science Technology Office, Greenbelt, MD 20771 USA.

Jeff D. Beck and William W. Sullivan III are with Leonardo DRS, Electro-Optical and Infrared Systems Dallas, Dallas, TX 75243 USA.

John E. Hubbs is with the U.S. Air Force Research Laboratory, Ball Aerospace and Technologies Corporation, Albuquerque, NM 87106 USA.

Color versions of one or more figures in this article are available at https://doi.org/10.1109/TNS.2020.3040741.

Digital Object Identifier 10.1109/TNS.2020.3040741

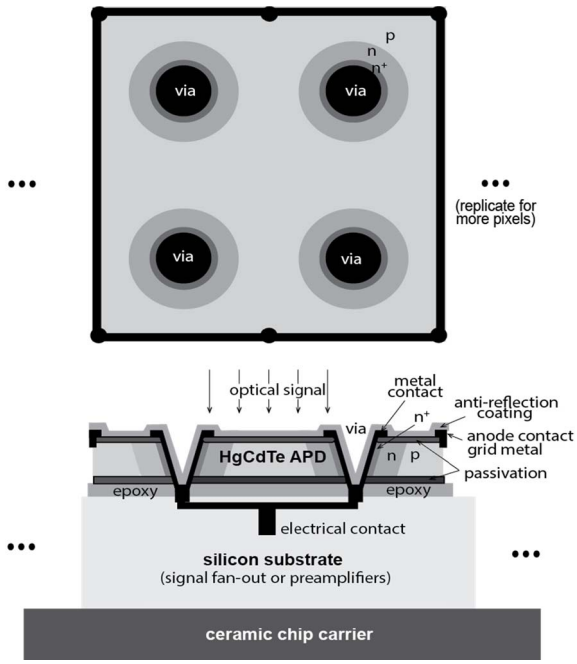

Fig. 1. Schematic of the HDVIP HgCdTe APD arrays by the Leonardo electro-optical infrared systems [33].

II. HgCdTe APD Array Design

Three types of HgCdTe APD arrays were tested: the 4×4 pixel APD fanout arrays with and without a wire-bonded read-out integrated circuit (ROIC) on the side and 2×8 pixel arrays that were vertically interconnected to ROIC preamp inputs directly under the APD array, as shown in Fig. 1 [33]. The HgCdTe APD arrays were fabricated by DRS using their high-density vertically integrated photodiode (HDVIP) design. The APD itself is a p-around-n cylindrical photodiode formed around the via that connects the HgCdTe diode to an input pad on the silicon substrate [4]–[6]. Four photodiodes in a 2×2 square pattern are connected in parallel to form a pixel. The devices we tested had either Hg-vacancy doping or both Cu- and Hg-vacancy doping on the p-side at around 1×10^{16} cm^{-3}. On the n-side, the indium donor doping was about 10^{14} cm^{-3} [4]. At high biases, the n-region becomes fully depleted and forms the high-field APD gain region. The 4.4-μm cutoff HgCdTe material used for these 4×4 and 2×8 pixel devices came from the same material lot with a split between p-type doping, with and without added copper. The ROICs for both types of devices were designed and fabricated by the same company (ADIC Inc., Longwood, FL) using the same foundry service (Jazz Semiconductor) and ROIC fabrication process. Therefore, the results from either device should apply to the other.

The 4×4 pixel devices use a fanout substrate and the cathodes of all pixels are brought to the side of the substrate and wire bonded to the ROIC on the same chip carrier. The cathodes of the APD are connected to the input terminals of the preamplifiers. The anodes of the APDs are the shared (common) p-type substrate which is connected to a metal substrate contact ring. The top-side contact ring surrounds the array and is connected to the detector bias voltage supply. The bias voltages for all pixels are identical. Both the APDs and the ROIC can be independently fabricated and tested before integration. The pixel size is 80 μm $\times$ 80 μm on an 80-μm pitch. A guard ring is included around the pixel array, which consists of identical APD diodes. The combined electrical bandwidth of the device was about 7 MHz, which was optimized for our CO_2 sounder lidar with 1-μs wide laser pulses [16].

The 2×8 pixel array has its ROIC inside the silicon substrate under the HgCdTe APD pixels to minimize the stray capacitance [17]. The electrical bandwidth is about 50 MHz [19]. Single-photon events can be detected when the APD gain is above 500 [17]–[19]. The pixel size is 64 μm $\times$ 64 μm on a 64-μm pitch. There are also a substrate contact ring and guard ring around the 2×8 pixel array.

III. Proton Radiation Damage of a 4×4 Pixel HgCdTe APD Array Without ROIC

A. Test Setup

A 4×4 pixel HgCdTe APD fanout array without an ROIC was first tested with protons at the Crocker Nuclear Laboratory (CNL), University of California, Davis, CA, on November 28–29, 2012. The test was conducted by personnel from the Infrared Radiation Effects Laboratory (IRREL), Air Force Research Laboratory (AFRL). The detector was housed in their low background noise liquid nitrogen Dewar similar to those used in other infrared FPA tests [25]. A block diagram of the test setup is shown in Fig. 2.

The test device had a Cu- and Hg-vacancy doping. All but three pixels of the test device had gain-normalized dark currents <1 pA. The tests were automated to measure the current versus voltage (I–V) curves of the four pixels with the lowest initial dark currents. The test device was oriented 45° from the incoming proton beam so that it could be illuminated with a light source from another window on the Dewar to measure the quantum efficiency and APD gain. All the measurements were performed with the device cooled to 80 K.

The proton energy was 63 MeV behind the Dewar window. The proton beam diameter was 70 mm, which is much larger than the APD array. The proton flux during the irradiation was approximately 4×10^7 cm^{-2} s^{-1} (8.3 rad(Si)/s ionizing dose rate). The HgCdTe APD array was not biased but grounded during the proton irradiation. The proton irradiation was applied in steps of 1, 2, 5, 10, 20, 30, 50, and 100 krad(Si) and the APDs were characterized upon each irradiation step. In this test setup with 63-MeV protons, each 1.0 krad(Si) ionization dose was equivalent to 7.5×10^9 cm^{-2} fluence on the detector. The device was measured again after warming up to room temperature overnight and cooling down again to 80 K the next day. The measurement was repeated back at IRREL/AFRL eight weeks after the test and again at DRS 12 weeks after the test. The device was at room temperature during transportation and storage.

B. Test Results

The measured dark currents from one of the four pixels as a function of the proton fluence and dose at 12-V APD

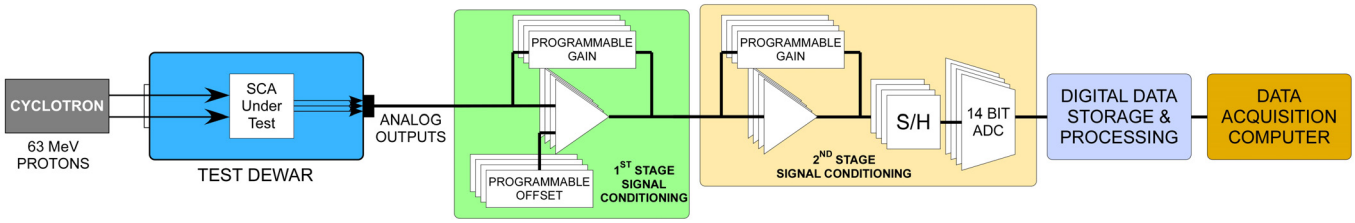

Fig. 2. Block diagram of the test setup of the proton irradiation of the HgCdTe APD arrays and performance monitoring by AFRL at CNL. (SCA: sender chip assembly; S/H: sample and hold; ADC: analog to digital converter).

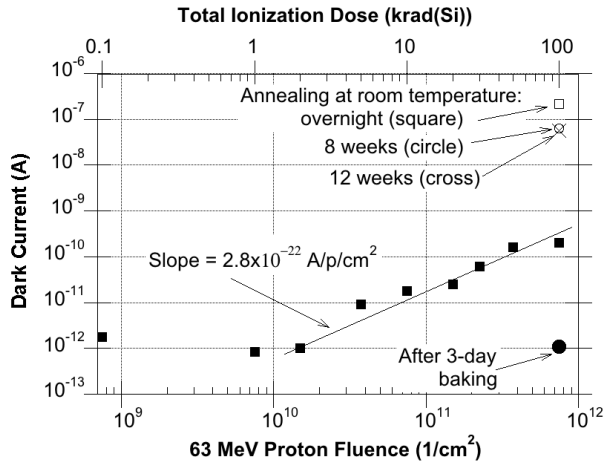

Fig. 3. Dark current versus proton fluence of the HgCdTe APD, pixel (3,4) at 12-V APD bias.

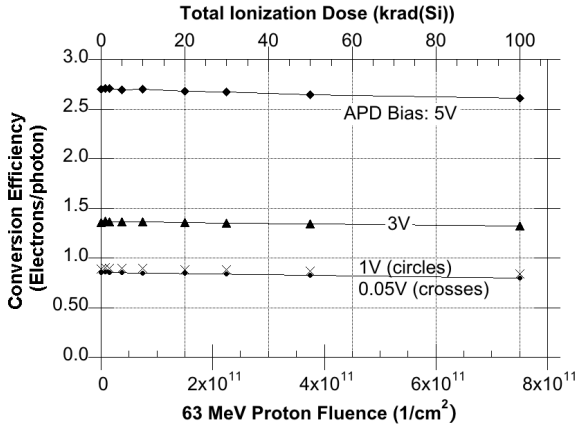

Fig. 4. APD photon-to-electron conversion efficiency (quantum efficiency times the gain) versus proton fluence of the HgCdTe APD, pixel (3,4), at several APD biases.

bias (gain ~650) are plotted in Fig. 3. The Dewar leakage current was about 0.3 pA and was lower than the APD dark currents being measured. The dark current increased roughly linearly with the proton fluence after 1 krad(Si). The rate of increase of all four pixels being measured is listed in Table I. The dark currents due to radiation damage increased with the APD bias and were roughly proportional to the APD gain, which indicates that the charges were generated in the p-side of the devices and multiplied by the APD gain.

The APD responsivity in terms of the output number of electrons per incident photon (product of the quantum efficiency and the APD gain) was monitored at several intermediate proton fluences with the APD biased at 0.05, 1, 3, and 5 V. The measurement results from one of the pixels are shown in Fig. 4. At APD bias of 0.05 V, the APD gain can be assumed as unity [5], [6] and the responsivity becomes the same as the APD quantum efficiency. The APD gain at other bias voltages can be obtained by dividing the responsivity at the given bias by that at unity gain (0.05 V bias).

There was a slight decrease (<6%) in the APD responsivity under a fixed illumination level at all APD biases. There was also a slight increase (~5%) in the APD gain at 5 V bias. All four pixels showed the same behavior.

An unexpected reverse annealing behavior was observed after warming up and cooling down again. The dark currents increased by two to three orders of magnitude. All four pixels measured exhibited similar behavior. The dark currents stayed nearly unchanged when measured again eight weeks later at IRREL/AFRL.

The dark currents remained high when measured again at DRS about 12 weeks after the proton irradiation. The APD gain and quantum efficiency were measured again and no measurable changes were observed. The small degradation in the APD quantum efficiency observed at CNL annealed out by the time that DRS recharacterized the device.

The device was then baked at 100 °C for 72 h and characterized again. Surprisingly, the dark currents returned to normal after the bake. Table I summarizes the results from the four pixels monitored at CNL. The rest of the pixels, besides the three defective ones and the three damaged during handling, all showed a 2–3 order-of-magnitude reduction in the dark currents following the bake.

IV. Proton Radiation Damage of a 4 × 4 Pixel HgCdTe APD Array With ROIC

A. Test Setup

A second proton radiation damage test was conducted on a 4 × 4 pixel HgCdTe APD array with the ROIC. The test was conducted again at CNL with 63-MeV protons using a similar test setup by IRREL/AFRL on September 16, 2013. The average proton flux was set to about 8.8×10^7 cm^{-2} s^{-1} (16.5 rad(Si)/s, about twice the rate of the first test), and the device was irradiated in several steps up to 30 krad(Si). The device temperature was held at 80 K during the proton irradiation and post irradiation characterization. The device was not biased but grounded during the irradiation.

TABLE I
DARK CURRENTS OF THE FOUR PIXELS OF THE 4 × 4 HgCdTe APD ARRAY WITHOUT ROIC AT 12-V APD BIAS

Pixel	Before Irradiation (A)	Rate of Increase[a] (A/proton/cm^2)	After 100 krad(Si) (A)	After warming to room temperature and cooling-down again (A)	After an 8-week storage at room temperature at AFRL (A)	After a 3-month storage at room temperature at DRS (A)	After a 72-hour bake at 100 C at DRS (A)
Pixel (3,4)	$1.81\ 10^{-12}$	$2.8\ 10^{-22}$	$1.80\ 10^{-11}$	$2.15\ 10^{-7}$	$6.30\ 10^{-8}$	$5.70\ 10^{-8}$	$1.09\ 10^{-12}$
Pixel (4,3)	$2.24\ 10^{-12}$	$7.2\ 10^{-22}$	$6.41\ 10^{-10}$	$2.00\ 10^{-7}$	$5.91\ 10^{-8}$	$5.85\ 10^{-8}$	$1.13\ 10^{-12}$
Pixel (1,4)	$2.06\ 10^{-12}$	$1.5\ 10^{-21}$	$1.00\ 10^{-9}$	$4.25\ 10^{-7}$	$7.80\ 10^{-8}$	$3.87\ 10^{-8}$	$7.54\ 10^{-13}$
Pixel (3,3)	$2.49\ 10^{-12}$	$9.8\ 10^{-22}$	$6.95\ 10^{-10}$	$2.57\ 10^{-7}$	$7.80\ 10^{-8}$	$4.80\ 10^{-8}$,[b]	-[c]
Median	$2.15\ 10^{-12}$	$8.5\ 10^{-22}$	$6.68\ 10^{-10}$	$2.36\ 10^{-7}$	$7.05\ 10^{-8}$	$5.25\ 10^{-8}$	$1.09\ 10^{-8}$

[a] Slope after the dark currents rose above the noise floor.
[b] Extrapolated from the data taken at 10 V APD bias.
[c] Pixel damaged due to handling, no post-bake measurement data available for the pixel.

The test device this time had a Hg-vacancy p-type doping. The APD dark and photo currents were measured through the ROIC operated in the capacitive transimpedance preamplifier (CTIA) mode. In this mode, the APD output current charges a capacitor and the ROIC outputs the voltage across the capacitor. The capacitor is periodically discharged via a reset switch. The rate of increase of the CTIA output voltage is proportional to the APD current. The CTIA gain was calibrated to be 2.4 μV/electron. The maximum APD current ROIC could measure was 130 pA. The standard deviation of the measurement noise after averaging was about 0.01 pA.

The outputs from the ROIC in resistive transimpedance amplifier (RTIA) mode were also monitored with the APD bias set to near zero to determine the RTIA noise floor and at nominal APD bias to determine the noise equivalent power (NEP) from the combination of the APD and the ROIC.

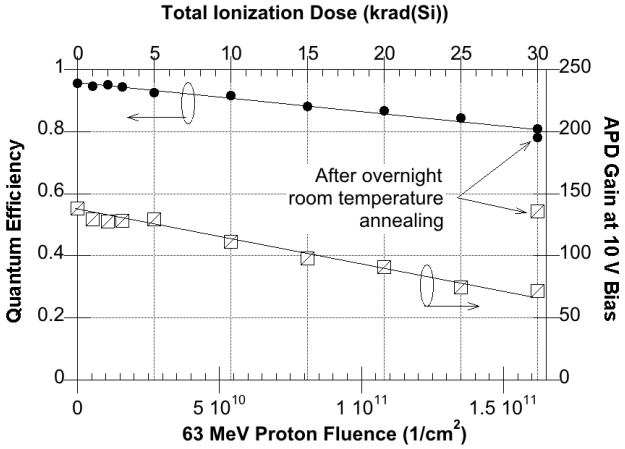

Fig. 5. APD median quantum efficiency and gain versus proton dose up to 30 krad(Si) at 10-V APD bias (APD gain ∼120). Note the near-complete recovery of the APD gain after annealing at room temperature overnight.

B. Test Results

The dark currents from all pixels were monitored at 10-V APD bias and several intermediate irradiation doses up to 30 krad(Si). Similar to the earlier test, the dark currents rose linearly with proton fluence after a few krad(Si) total dose. The rate of increase in the radiation-induced dark currents was about the same as that from the earlier test without the ROIC.

The dark currents from all pixels were measured again after warming up the device overnight and cooling it down again. They all increased by at least a factor of 10 and were beyond the linear dynamic range of the CTIA outputs. This result confirmed the reverse annealing effect observed during the first test.

The APD responsivities at 0.05, 1.0, 2.5, 5.0, 7.5, and 10 V bias were also measured after each proton dose and after overnight room-temperature annealing using a blackbody source and a chopper. Fig. 5 shows the median of the APD quantum efficiency and gain at 10 V bias. The quantum efficiency, which is the same as the responsively at 0.05 V bias, decreased linearly with the proton fluence by 18% at 30 krad(Si). It did not change significantly after room-temperature annealing. Based on earlier studies, this decrease could be the result of the reduction of the minority carrier lifetime from the radiation damage [25]. The responsivity at higher APD bias is the product of the quantum efficiency, the APD gain, and the CTIA gain. Assuming the CTIA gain was unchanged, the APD gain decreased by more than a factor of 2 at 30 krad(Si) but largely recovered after warming up to room temperature overnight (Fig. 5). Compared to the first test, the APD gain in this case decreased much faster immediately after the irradiation. Some of the differences may be attributed to the difference in the dose rate of protons and/or doping of HgCdTe APDs. The 4 × 4 fanout device used in the first test was Cu- and Hg-vacancy doped and the fanout/ROIC device in the second test was only Hg-vacancy doped.

There was no change observed in the RTIA output noise when the APD was biased to 0.05 V (unity APD gain) up to 30 krad(Si). We also tested an ROIC chip without the HgCdTe APD to 100 krad(Si) at room temperature with all the terminals grounded. The ROIC chip was reevaluated back at ADIC Inc., two months after the irradiation. There were no measurable changes in the ROIC performance. However, radiation damage of the ROIC still could not be ruled out since silicon devices are known to suffer total ionization damage when biased during irradiation, especially when operating at lower temperatures.

The post-irradiation tests at DRS showed that the APD dark currents were about the same as those last measured at CNL and IRREL/AFRL. There was little annealing in the dark current at room temperature over the 2.5-month

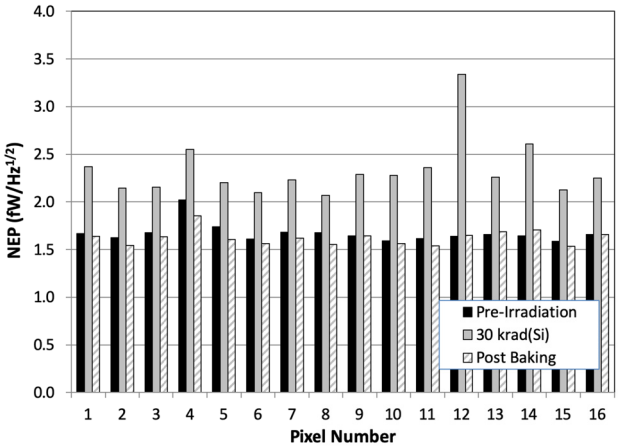

Fig. 6. NEPs of the HgCdTe APD before and after a 30 krad(Si) proton irradiation. The NEPs returned to the preirradiation levels after a 72-h 90 °C bake out.

period. However, the quantum efficiencies, which decreased by about 18% after the proton irradiation, largely annealed to the original level after the 2.5-month storage at room temperature.

The dark currents from all the pixels returned to the pre-irradiation level after baking the device at 90 °C bake for 72 h. The APD quantum efficiency and the gain also returned to the pre-irradiation values within the measurement uncertainty after the bake.

The RTIA output noise levels were remeasured back at DRS. It confirmed that the ROIC noise with the APD at unity gain was unchanged from the preirradiation level. The RTIA output noise at 10-V APD bias (gain ∼150) increased significantly because of the much elevated APD dark currents and the post-irradiation reverse annealing effect. Fig. 6 shows the NEP spectral density obtained by dividing the pixel output spectral noise density in $V/Hz^{1/2}$ by the APD-ROIC responsivity in V/W. Similar to APD dark currents, the NEPs annealed out after baking at 90 °C for 72 h.

The transient response of the device was tested by setting the APD bias to 10 V and lowering the proton flux such that each pixel was hit by a proton once a few seconds. The ROIC was operated in CTIA mode during this test. The APD produced a large current pulse in response to each proton hit, which mostly saturated the CTIA ($\sim 10^6$ electrons dynamic range). Considering the APD gain (∼150), each proton hit on average produced $\gg 10^4$ electrons within the APD active volume where photoelectrons are generated and multiplied by the APD gain. The ROIC output often latched up to its maximum level upon a proton hit, which could be cleared by power cycling the device.

We later reproduced the phenomenon with strong laser pulses in our lab. Upon latch-up, the APD current increased sharply by about a factor of 10, while other power supply currents to the ROIC remained in their nominal range. Latch-up could be cleared by lowering the APD bias to below 3 V. We also found that latch-ups only occurred when the guard diodes were shorted, as they did during the test at CNL. No latch-ups were observed after the guard diodes were reversely biased. Based on these lab tests, we believe latch-ups observed during proton irradiation were caused by the APD but not the ROIC. The most likely cause was minority carrier injection breakdown from guard diodes which can produce a nonohmic injection contact close to the APD gain region and cause a self-sustained high APD current. This type of latch-up can be avoided by keeping the guard diodes reverse-biased.

The ROIC, which consists of transimpedance amplifiers (TIAs) and the associated CMOS logic circuitry, may still be susceptible to single-event latch-up (SEL) or other single-event effects (SEEs) from more energetic particles in space [34], [35]. Nevertheless, these test results showed SEL due to protons is unlikely at our operational temperature (80 K). We also plan to remove all CMOS logic circuits in the ROIC in future devices. The logic circuit in the current ROIC is for TIA gain setting and RTIA to CTIA switching, which are not necessary for our lidar applications.

V. Gamma-Ray Radiation Damage of a 4 × 4 Pixel HgCdTe APD Array Without ROIC

A. Test Setup

One Cu- and Hg-vacancy-doped HgCdTe APD array without ROIC was irradiated with gamma rays using a ^{60}Co test source on October 21, 2015. Unlike protons, gamma rays are known to cause mostly ionization damage but little displacement damage. The objective of the test was to investigate whether the HgCdTe APDs were susceptible to ionization damage and how much of the radiation damage from the proton irradiation could be attributed to ionization damage.

The device was held at 80 K during the irradiation and post-irradiation characterization. An aluminum blank was placed in front of the test device and held at 80 K to block the incident light and minimize ambient thermal emission on the detector. The APD I–V curves from five pixels were measured with a picoampere meter and a power supply. The leakage currents of this test setup were much higher than those with the IRREL/AFRL test system but still below the dark current of HgCdTe APDs when biased above 7 V.

The gamma-ray ionizing dose rate was set to 10 rad(Si)/s, comparable to that during the proton radiation tests. The cathodes and the anodes of the APDs were shorted to ground during the irradiation. The I–V curves of the device were measured after 2, 5, 10, 20, 30, 50, and 100 krad(Si) doses.

B. Results From the Gamma-Ray Test

There was no apparent change in the APD dark currents after gamma-ray irradiation up to 100 krad(Si). The APD dark currents and the gain were remeasured back at DRS 1.5 months after the gamma-ray irradiation using their low leakage current and low background measurement system. There were no measurable changes compared to preirradiation measurements. The gamma-ray radiation damage to the HgCdTe APDs, if any, had been annealed out during the 1.5-month room-temperature storage and transport. These results indicate that the HgCdTe APDs are likely not susceptible to ionization damage up to 100 krad(Si) though another test with the device fully biased is needed before we can reach a definite conclusion.

VI. Proton Radiation Damage of 2 × 8 Pixel HgCdTe APD Arrays With ROIC

A. Test Setup

A third proton radiation damage test was performed on two 2 × 8 pixel HgCdTe APD arrays with the built-in ROIC. One device was Hg-vacancy-doped and the other one was Cu- and Hg-vacancy-doped. The diodes in the guard ring in these 2 × 8 pixel devices were reversely biased this time. The ROIC consisted of a set of low-noise RTIA preamplifiers, one for each pixel. When the APDs were biased at 12 V, the devices were capable of detecting single-photon events as well as individual electrons from the APD bulk dark current. The purpose of this proton irradiation test was to: 1) measure the detector transient response to single proton events; 2) compare the radiation damage of 2 × 8 and 4 × 4 pixel HgCdTe APDs; 3) verify no latch-ups when the guard diodes were reversely biased; and 4) find a lower baking temperature and the minimum baking time to anneal the radiation damage.

The test was conducted at CNL on August 28, 2017. The APD arrays were placed inside a liquid nitrogen Dewar with the cold filter replaced with an aluminum blank. The detector chip was oriented normal to the incoming proton beam. The device was held at 80 K during proton irradiation and postirradiation characterization. A small heater was attached to the cold finger and a closed-loop controller was used to heat the device during annealing.

The proton energy on the detectors was about 55 MeV considering the attenuation by the Dewar window and the aluminum blank in front of the detector. The test started at a relatively low proton flux, about 10^5 cm^{-2} s^{-1}, so that the detector response from individual proton hits could be distinguished on an oscilloscope. The ROIC was powered and the APD gain was gradually increased after the irradiation started to determine the effect of the APD gain on the output pulse amplitude. Each detector was irradiated for tens of minutes at the highest APD gain (12 V bias) to ensure the detectors survived the transient proton hits expected in space.

The proton flux was then increased to 2.5 × 10^7 cm^{-2} s^{-1} for accumulated dose tests of 2, 5, and 10 krad(Si) with the devices powered off. The temperature of the devices returned to room temperature after the liquid nitrogen boiled off overnight. The dark currents were measured again after cooling down to 80 K to find if these 2 × 8 pixel devices also exhibited reverse annealing. The devices were then heated and cooled again for several cycles to determine the optimal temperature and duration for annealing. One of the devices was irradiated again with power on by another 10 krad(Si) (total 20 krad(Si), or 1.5 × 10^{11} cm^{-2} fluence of 55-MeV protons) after it was fully annealed. The proton flux was about 3 × 10^6 cm^{-2} s^{-1} during this part of the test. The dark count rates were measured again at GSFC about a month later through several heating–cooling cycles until they returned to the preirradiation levels.

B. Transient Effects

Large-amplitude pulses were observed from the detector outputs when irradiated by low-flux protons. The pulse shapes were similar to those under strong optical input. The rate of these large pulses from each pixel corresponded roughly to the proton hit rate per pixel. The pulse amplitude and degree of saturation increased with the APD bias, as shown in Fig. 7. At 0-V APD bias, the output was mostly unsaturated and the median pulse amplitude was about 120 mV. Considering the losses of the long coax cable (1 dB) and the power splitter (3 dB) between the oscilloscope and the rest of the test equipment, the actual median pulse amplitude should have been 190 mV. Since the mean single-photon pulse amplitude for this device is 37 mV at an APD gain of 1100 [18], or 0.034 mV at unity gain, each proton hit on average produced approximately 5600 electrons at unity APD gain. The rebounds in the tails of pulse waveforms when the pulses started to saturate are believed to be an artifact of the ROIC since they increased with the APD bias voltage and hence the input pulse amplitude to the ROIC. The tails of the pulse waveform changed shape when the ROIC became more deeply saturated.

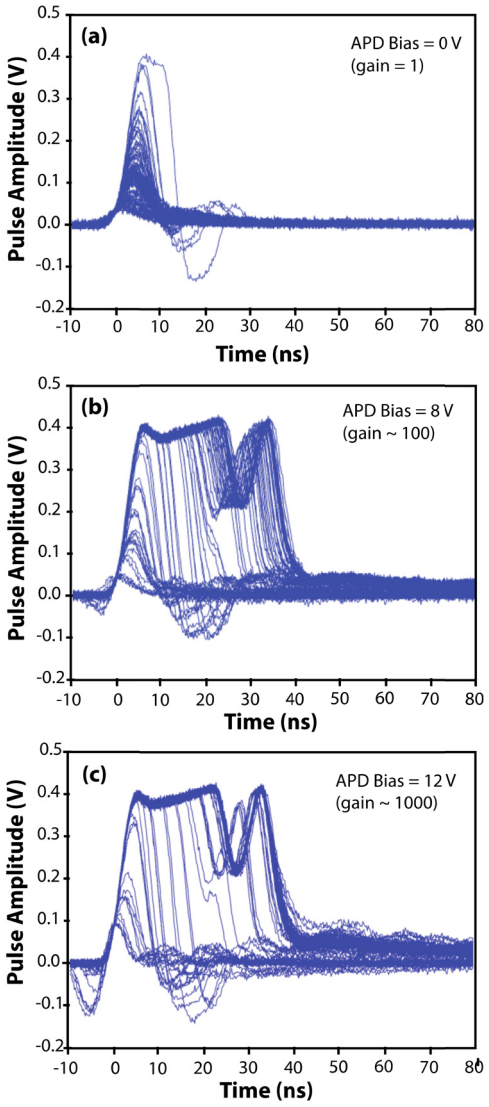

Fig. 7. Sample HgCdTe APD output pulse waveforms in response to proton hits with the APD biased at (a) 0 V; (b) 8 V; and (c) 10 V.

Fig. 8 shows the same pulse waveforms at 12-V APD bias but over a much longer time period to measure the recovery

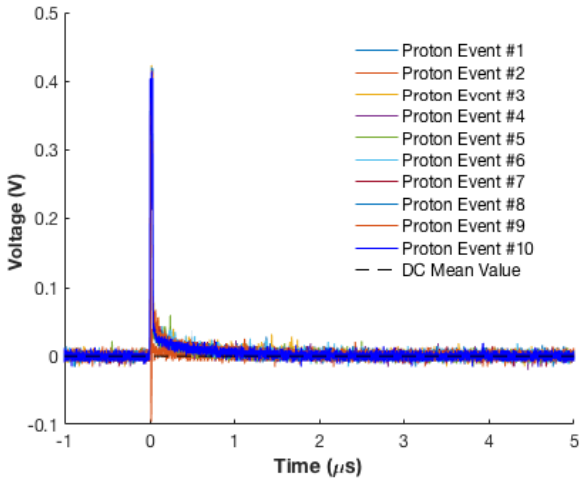

Fig. 8. Sample HgCdTe APD output pulse waveforms in response to proton hits with the APD biased at 12 V [33].

time. The detector outputs returned to the original level after about 1 μs. There were sometimes negative going spikes in the output waveforms, which are believed to be caused by a proton hit on the adjacent pixel, causing a temporary dip in the bias voltage for the nearby diodes. All pixels functioned nominally without permanent damage. There was no latch-up during these tests with the guard diodes reversely biased. There was also no CMOS digital circuit in this ROIC.

C. Accumulated Proton Radiation Damage and Annealing After High Temperature Bake

Like in the earlier tests with the 4 × 4 pixel devices, both the 2 × 8 pixel devices started to show significant radiation damage after being irradiated by protons at high flux to 10 krad(Si). The APD dark count rate increased significantly after warming up the devices to room temperature overnight.

We first baked one device at 70 °C for an hour but observed little change in the dark count rate. We then raised the temperature to 85 °C and baked for 1.5 h and observed noticeable annealing. The dark count rates returned to the preirradiation levels after baking at 85 °C for a total of 3 h for the Hg-vacancy-doped device and 4.5 h for the Cu- and Hg-vacancy-doped device.

Fig. 9 shows the dark count rates versus threshold voltage for the Hg-vacancy-doped devices before and after the proton irradiation and after baking [33]. The measured dark counts at <50 mV threshold were mostly caused by the electronic noise of the ROIC, whereas the dark counts at >50 mV threshold were mostly caused by the APD dark current. Only a few pixels showed increased dark count rate at 10 krad(Si) when the devices were kept at 80 K. However, the damage extended to almost all the pixels after warming up to room temperature and cooling down again. The Cu- and Hg-vacancy-doped device showed similar behavior.

The dark count rates of the device with the second 10 krad(Si) dose exhibited similar behavior. The silicon ROIC performed nominally and no difference was observed in the second test while powered.

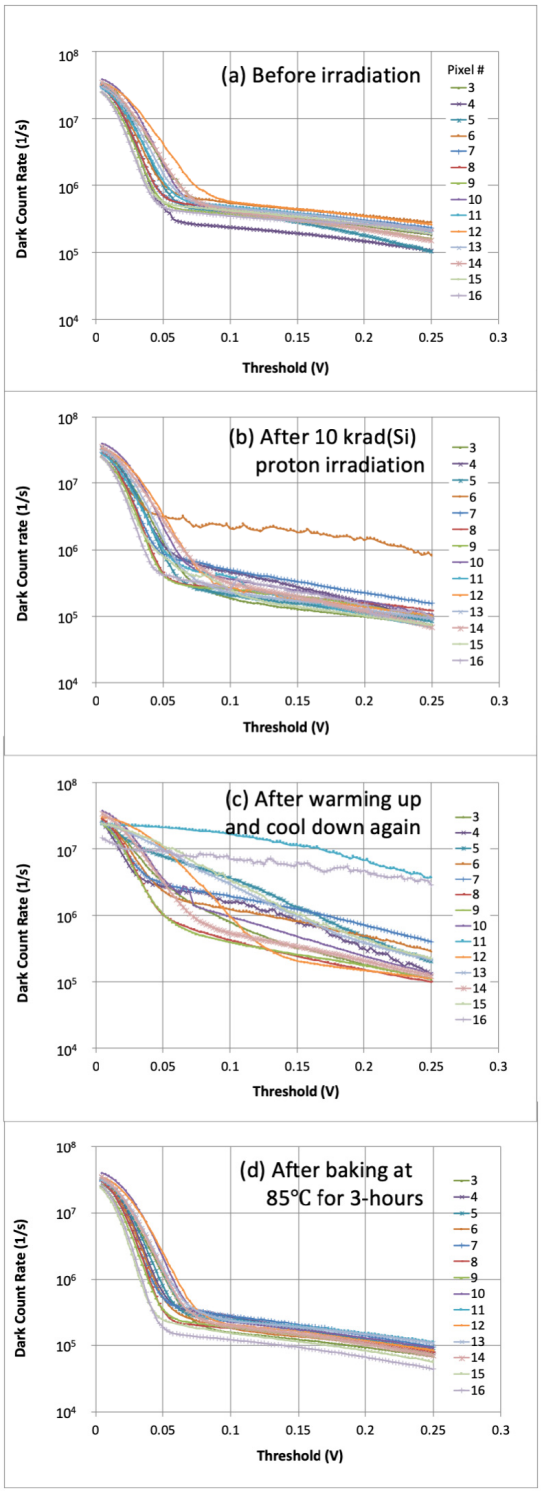

Fig. 9. HgCdTe APD dark count rates versus threshold from the Cu–Hg-doped device. (a) Before proton irradiation. (b) After 10-krad(Si) proton irradiation. (c) After warming up to room temperature overnight. (d) After a 3-h 85 °C bake. The data were from the Hg-vacancy-doped device. The Cu–Hg-doped device showed similar behavior. The measurements were taken with a universal counter with the device at 80 K [33].

Fig. 10 shows a history of the dark count rates of the Hg-vacancy-doped device at 100 mV threshold for the entire test period. The postirradiation measurements confirmed the device started to suffer significant proton radiation damage

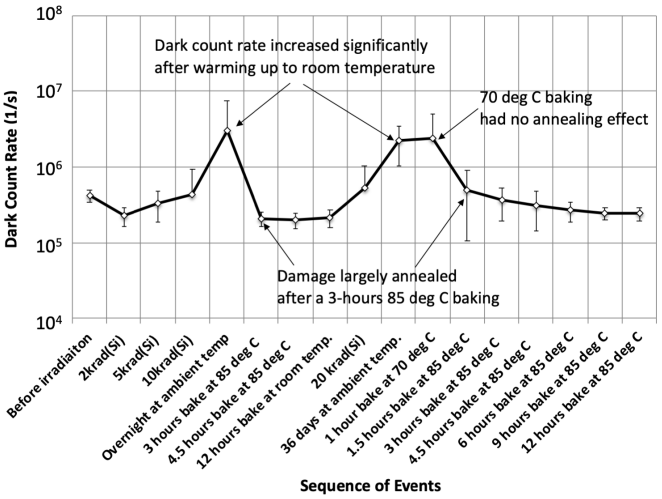

Fig. 10. 2 × 8 pixel HgCdTe APD median dark count rates at a threshold setting of 100 mV through the sequence of events of proton irradiation and annealing. The data are from the Hg-vacancy-doped device [33].

after 10 krad(Si). A baking temperature of 70 °C was not effective and 85 °C was required for effective annealing. A longer baking time (12 h) was needed this time for the dark count rate to return to the original level compared to 3 h after the initial 10 krad(Si) irradiation. The need for a longer baking time might be caused by the fact that the device was biased during the second 10 krad(Si) irradiation.

The APD responsivity was checked using a pulsed laser at GSFC before the proton irradiation and after the last high-temperature bake. No measurable degradation was found. Radiation damage in the APD responsivity, if any, was annealed by the high-temperature bake, as in the first two proton tests.

VII. Space Applications and Radiation Damage Mitigation

The purpose of this study was to assess whether the HDVIP-type HgCdTe APD arrays can be used in space lidar. For a typical Earth orbiting mission, the primary radiation sources are solar protons and protons trapped in Earth's magnetic field that have energies up to several 100 MeV [32]. Trapped electrons with energies up to 10 MeV are also a concern. In detectors, protons and electrons can cause displacement and ionization damage, respectively.

In a typical space lidar, detectors are usually well shielded by the optics, coolers, and other structures. As an example, a 3-D ray-tracing analysis for the Ice, Cloud, and land Elevation Satellite (ICESat) mission showed the lidar detectors on ICESat in a circular polar orbit at ∼600 km altitude had an estimated dose of <5 krad(Si) over a five-year mission. The majority of the radiation emerging from the shielding materials is protons from a few to several 100 MeV at an integral fluence of about 10^{10} cm^{-2}. The peak flux was estimated to be about 1000 cm^{-2} s^{-1}, or an average of about 0.04 proton hits/pixel/s. For a typical planetary mission (with the exception of missions to the Jovian system), the major source of radiation is the solar protons and electrons and the total fluence at the lidar detectors is similar to that from trapped and solar protons in a polar Earth orbiting mission.

The results from our proton and gamma-ray tests show that it is feasible to use these HgCdTe APD arrays in space. The devices can continuously operate under proton radiation. Transient proton hits produce large electrical pulses, but recover within 1 μs and only interrupt a few lidar measurements. Accumulated proton radiation effects can be annealed, when required, by heating the devices at 85 °C for several hours.

The APD gain appeared to have little change for the Cu- and Hg-vacancy-doped devices up to 100 krad(Si) but decreased by almost 20% by 30 krad(Si) for the Hg-vacancy-doped devices. A small decrease in the APD gain like this can be compensated by increasing the APD bias. Latch-ups of the HgCdTe APDs can be avoided by keeping all the guard diodes fully reverse-biased.

An unexpected phenomenon was that radiation damage caused the APD dark current to increase by two to three orders of magnitude after the detector was brought to room temperature and cooled down again. Based on this finding, the lidar detector should be kept at cryogenic temperature and power cycling of the cooler should be avoided whenever possible.

The physics of the proton-induced degradation mechanism and the short-term and long-term annealing behavior are not very well understood at present. One hypothesis is that proton bombardment breaks the chemical bonds between the Group II metal site atoms, Cd and Hg, and the Group VI atoms (tellurium). This may cause Cd and Hg atom displacement and the creation of metal site vacancies, which are known to degrade the electron minority carrier lifetime and, hence, the electron diffusion length on the p-side of the junction. This hypothesis would explain the decrease in gain and quantum efficiency and increase in dark current during proton irradiation. However, the magnitude of the dark current increase after warming up to room temperature and cooling down cannot be explained by a simple bulk lifetime degradation and suggests that a surface effect may also be occurring. One possible explanation is that when the HgCdTe APDs are warmed up upon proton irradiation, the crystal matrix relaxes and additional defect sites (vacancies) are created, causing the reverse annealing. After heating at elevated temperatures, the bulk and surface of the HgCdTe materials return to their thermal equilibrium state and the defects are annealed out. Further studies are needed to fully understand the physics of these radiation damage and annealing behaviors.

VIII. Conclusion

The proton radiation effect on several Leonardo DRS Electro-Optical Infrared Systems HgCdTe HDVIP APD detector arrays was characterized. The detectors produced a large current pulse in response to each proton hit but recovered within 1 μs. The most significant long-term effect was the increase of the APD dark current. Furthermore, the dark current due to radiation damage increased by two to three orders of magnitude after the devices were brought to room temperature and cooled down again. However, all radiation damage could be annealed out by heating the device to

85 °C for several hours. The devices are feasible for use in a space lidar in a typical multiyear Earth and planetary science mission provided they can be heated periodically to anneal out radiation damage when it started to impact the lidar receiver performance.

ACKNOWLEDGMENT

The authors would like to thank Infrared Radiation Effects Laboratory (IRREL)/Air Force Research Laboratory (AFRL) for planning and conducting the first two proton radiation tests. They would like to thank the Crocker Nuclear Laboratory (CNL) for facilitating the test, Dr. Isaak Samsel, formerly NASA Goddard Space Flight Center (GSFC), for the support of the third proton radiation test, James McCurdy of DRS for modifying the Dewar system to allow heating the device in the Dewar, and NASA Earth Science Technology Office for supporting this work.

REFERENCES

[1] A. Waczynski *et al.*, "HgCdTe detectors for the Hubble space telescope wide field camera 3 IR channel," in *Scientific Detectors for Astronomy*, P. Amico, J. W. Beletic, and J. E. Beltic, Eds. New York, NY, USA: Springer, 2004, pp. 175–182.

[2] B. Rauscher *et al.*, "New and better detectors for the JWST near-infrared spectrograph," *Astronomical Soc. Pacific*, vol. 126, pp. 739–749, Aug. 2014.

[3] B. J. Rauscher, "An overview of detectors (with a digression on reference pixels," in *Proc. JWST NIRSpec HAWAII-2RG, STSci Calibration Workshop*, Baltimore, MD, USA, Jul. 2010, p. 167. Accessed: Dec. 13, 2020. [Online]. Available: https://jwst.nasa.gov/content/about/innovations/infrared.html

[4] J. Beck *et al.*, "The HgCdTe electron avalanche photodiode," *J. Electron. Mater.*, vol. 35, no. 6, pp. 1166–1173, Jun. 2006.

[5] M. A. Kinch, *Fundamental of Infrared Detector Materials*. Bellingham, WA, USA: SPIE, 2007, ch. 7.

[6] M. A. Kinch, *State-of-the-Art Infrared Detector Technology*. Bellingham, WA, USA: SPIE, 2014, ch. 6.

[7] I. Baker and M. Kinch, "HgCdTe electron avalanche photodiodes (EAPDs)," in *Mercury Cadmium Telluride: Growth, Properties and Applications*, P. Capper and J. Garland, Eds. Chichester, U.K.: Wiley, 2011, ch. 21.

[8] G. Finger *et al.*, "Evaluation and optimization of NIR HgCdTe avalanche photodiode arrays for adaptive optics and interferometry," *Proc. SPIE*, vol. 8453, Sep. 2012, Art. no. 84530T.

[9] D. E. Atkinson, D. N. B. Hall, S. M. Jacobson, and I. M. Baker, "Dark current in the SAPHIRA series of APD arrays," *Astronomical J.*, vol. 154, no. 6, p. 265, Nov. 2017.

[10] D. Atkinson, D. Hall, S. Jacobson, and I. M. Baker, "Photon-counting properties of SAPHIRA APD arrays," *Astronomical J.*, vol. 155, no. 5, p. 220, May 2018.

[11] I. M. Baker *et al.*, "Linear-mode avalanche photodiode arrays in HgCdTe at Leonardo, U.K.: The current status," *Proc. SPIE* , vol. 10980, May 2019, Art. no. 109800K.

[12] J. Rothman, L. Mollard, S. Goüt, L. Bonnefond, and J. Wlassow, "History-dependent impact ionization theory applied to HgCdTe e-APDs," *J. Electron. Mater.*, vol. 40, no. 8, pp. 1757–1768, Jun. 2011.

[13] A. Dumas *et al.*, "Evaluation of a HgCdTe e-APD based detector for 2 μm CO_2 DIAL application," *Appl. Opt.*, vol. 56, no. 27, pp. 7577–7585, Sep. 2017.

[14] M. Jack, J. Wehner, J. Edwards, G. Chapman, D. N. B. Hall, and S. M. Jacobson, "HgCdTe APD-based linear-mode photon counting components and LADAR receivers," *Proc. SPIE*, vol. 8033, Jul. 2011, Art. no. 80330M.

[15] J. Beck, T. Welch, P. Mitra, K. Reiff, X. Sun, and J. Abshire, "A highly sensitive multi-element HgCdTe e-APD detector for IPDA lidar applications," *J. Electron. Mater.*, vol. 43, no. 8, pp. 2970–2977, May 2014.

[16] X. Sun, J. B. Abshire, J. D. Beck, P. Mitra, K. Reiff, and G. Yang, "HgCdTe avalanche photodiode detectors for airborne and space-borne lidar at infrared wavelengths," *Opt. Exp.*, vol. 25, no. 14, pp. 16589–16602, Jul. 2017.

[17] J. D. Beck *et al.*, "Linear mode photon counting with the noiseless gain HgCdTe e-avalanche photodiode," *Opt. Eng.*, vol. 53, no. 8, Apr. 2014, Art. no. 081905.

[18] W. Sullivan *et al.*, "Linear-mode HgCdTe avalanche photodiodes for photon-counting applications," *J. Electron. Mater.*, vol. 44, no. 9, pp. 3092–3101, May 2015.

[19] X. Sun *et al.*, "HgCdTe avalanche photodiode array detectors with single photon sensitivity and integrated detector cooler assemblies for space applications," *Proc. SPIE*, vol. 58, no. 6, Jun. 2019, Art. no. 067103.

[20] P. G. Lucey, X. Sun, J. B. Abshire, and G. A. Neumann, "An orbital lidar spectrometer for lunar polar compositions," in *Proc. 45th Lunar Planet. Sci. Conf. (LPSC)*, 2014, pp. 1–2, paper 2335. [Online]. Available: https://www.hou.usra.edu/meetings/lpsc2014/pdf/2335.pdf

[21] P. W. Marshall *et al.*, "Proton-induced transients and charge collection measurements in a LWIR HgCdTe focal plane array," *IEEE Trans. Nucl. Sci.*, vol. 50, no. 6, pp. 1968–1973, Dec. 2003.

[22] M. E. McKelvey *et al.*, "Radiation environment performance of JWST prototype FPAs," *Proc. SPIE*, vol. 5167, pp. 223–234, Jan. 2004.

[23] J. C. Pickel *et al.*, "Transient radiation effects in ultra-low noise HgCdTe IR detector arrays for space-based astronomy," *IEEE Trans. Nucl. Sci.*, vol. 52, no. 6, pp. 2657–2663, Dec. 2005.

[24] A. Waczynski *et al.*, "Radiation induced luminescence of the CdZnTe substrate in HgCdTe detectors for WFC3," *Proc. SPIE*, vol. 5902, Aug. 2005, Art. no. 59020P.

[25] J. E. Hubbs *et al.*, "Lateral diffusion length changes in HgCdTe detectors in a proton environment," *IEEE Trans. Nucl. Sci.*, vol. 54, no. 6, pp. 2435–2443, Dec. 2007.

[26] A. Weber *et al.*, "Radiation hardness of two-dimensional focal plane detector arrays for LWIR/VLWIR space sounding missions," in *Proc. 12th Eur. Conf. Radiat. Effects Compon. Syst.*, Sep. 2011, pp. 336–339.

[27] J. D. Bergeson, R. Bommena, S. Fahey, V. Cowan, C. Morath, and S. Velicu, "Mid and long wavelength infrared HgCdTe photodetectors exposed to proton radiation," *Proc. SPIE*, vol. 9226, Sep. 2014, Art. no. 92260P.

[28] M. L. Dorn *et al.*, "Proton irradiation results for long-wave HgCdTe infrared detector arrays for near-Earth object camera," *J. Astronomical Telescopes, Instrum., Syst.*, vol. 2, no. 3, Aug. 2016, Art. no. 036002.

[29] J. C. Pickel, A. H. Kalma, G. R. Hopkinson, and C. J. Marshall, "Radiation effects on photonic imagers—A historical perspective," *IEEE Trans. Nucl. Sci.*, vol. 50, no. 3, pp. 671–688, Jun. 2003.

[30] Y. Chang and S. Velicu, "High energy neutron irradiation effects on molecular beam epitaxy HgCdTe-based focal plane arrays and cameras," *Proc. SPIE*, vol. 10980, May 2019, Art. no. 109800V.

[31] J. Boldt, J. W. Alexander, H. Becker, E. Blazejewski, and E. H. Darlington, "Assessment of radiation effects on science and engineering detectors for the JEO mission study," Jupiter Europa Orbiter Mission Study, Pasadena, CA, USA, Tech. Rep. JPL D-48256, Nov. 2008.

[32] E. G. Stassinopoulos and J. P. Raymond, "The space radiation environment for electronics," *Proc. IEEE*, vol. 76, no. 11, pp. 1423–1442, Nov. 1988.

[33] X. Sun, J. B. Abshire, J.-M. Lauenstein, W. Sullivan, J. Beck, and J. E. Hubbs, "Evaluation of space radiation effects on HgCdTe avalanche photodiode arrays for lidar applications," *Proc. SPIE*, vol. 106240G, May 2018, Art. no. 106240G.

[34] C. J. Marshall *et al.*, "Mechanisms and temperature dependence of single event latchup observed in a CMOS readout integrated circuit from 16–300 K," *IEEE Trans. Nucl. Sci.*, vol. 57, no. 6, pp. 3078–3086, Dec. 2010.

[35] C. Virmontois *et al.*, "Dose and single-event effects on a color CMOS camera for space exploration," *IEEE Trans. Nucl. Sci.*, vol. 66, no. 1, pp. 104–110, Jan. 2019.